Conformational Exchange in Pseudoazurin: Different Kinds of Microsecond to Millisecond Dynamics Characterized by Their pH and Buffer Dependence Using ^{15}N NMR Relaxation†

Mathias A. S. Hass,‡,§ Monica D. Vlasie,|| Marcellus Ubbink,|| and Jens J. Led*,‡

Department of Chemistry, University of Copenhagen, Universitetsparken 5, DK-2100 Copenhagen Ø, Denmark, and Institute of Chemistry, Leiden University, Einsteinweg 55, 2333 CC Leiden, The Netherlands

Received October 1, 2008; Revised Manuscript Received November 16, 2008

ABSTRACT: The dynamics of the reduced form of the blue copper protein pseudoazurin from *Alcaligenes faecalis* S-6 was investigated using ^{15}N relaxation measurements with a focus on the dynamics of the micro- to millisecond time scale. Different types of conformational exchange processes are observed in the protein on this time scale. At low pH, the protonation of the C-terminal copper-ligated histidine, His81, is observed. A comparison of the exchange rates in the presence and absence of added buffers shows that the protonation is the rate-limiting step at low buffer concentrations. This finding agrees with previous observations for other blue copper proteins, e.g., amicyanin and plastocyanin. However, in contrast to plastocyanin but similar to amicyanin, a second conformational exchange between different conformations of the protonated copper site is observed at low pH, most likely triggered by the protonation of His81. This process has been further characterized using CPMG dispersion methods and is found to occur with a rate of a few thousands per second. Finally, micro- to millisecond motions are observed in one of the loop regions and in the α-helical regions. These motions are unaffected by pH and are unrelated to the conformational changes in the active site of pseudoazurin.

Pseudoazurin (PAZ)[1] belongs to the family of blue copper proteins. It functions as an electron donor for the copper-dependent nitrite reductase (NIR). The copper ion in the active site of PAZ is ligated by the side chains of His40, His81, Met86, and Cys89, assuming a distorted tetrahedral configuration (*1*). The copper binding imidazole group of His81 protrudes through the hydrophobic interface that binds to the NIR where it is thought to facilitate the electron transfer to NIR.

In reduced PAZ, His81 becomes protonated under acidic conditions and dissociates from the Cu(I) ion (*2*). As a consequence of this, the configuration of the Cu(I) ion changes from distorted tetrahedral to trigonal planar (*1*, *3*) and the protein becomes inactive (*2*). Similar acid transitions have been observed for other blue copper proteins, including amicyanin (*4*, *5*), stellacyanins (*6*), mavicyanin (*7*), and plastocyanin (PCu) (*3*, *8*). For both amicyanin and PCu, it has been found that the acid transition occurs on the microsecond time scale (*5*, *9*), and it has been suggested that this transition may regulate the biologic activity of these proteins (*10*, *11*). Therefore, information about the dynamics and kinetics of the acid transition may provide insight into the function of the copper site in blue copper proteins.

Here, we study the dynamics of PAZ from *Alcaligenes faecalis* (*Af*) S-6 to gain insight into the dynamics of the active site. Previously, ^{15}N NMR relaxation studies in combination with chemical shift analyses (*12*) have proved to be an efficient approach to studying the mechanism of the protonation of C-terminal copper-binding histidine in PCu, which is a close relative of pseudoazurin. Here, we apply the same approach to pseudoazurin from *A. faecalis* S-6 in investigating the dynamics on the microsecond time scale of His81 and the copper site of the protein. The studies show many similarities with PCu. However, striking differences are also revealed. These include an additional conformational exchange process at the copper site or in its vicinity at low pH, which is not observed in PCu, yet a similar conformational exchange has been observed for amicyanin (*5*). Thus, even though all three proteins function as electron transporters, the detailed molecular mechanism that leads to the function may vary among the proteins.

† This work was financially supported by Danish Agency for Science, Technology and Innovation Grants 9400351, 9801801, 26-03-0055, 21-04-0519, and 272-07-0466, Carlsbergfondet Grant 1624/40, Novo Nordisk Fonden Grant 2003-11-28, and Villum Kann Rasmussen Fonden Grant 8.12.2003. M.D.V. and M.U. were supported by The Netherlands Organisation for Scientific Research, Grant 700.52.425 (VIDI program).

* To whom correspondence should be addressed: Department of Chemistry, University of Copenhagen, Universitetsparken 5, DK-2100 Copenhagen, Denmark. Telephone: (+45) 3532 0325. Fax: (+45) 3535 0609. E-mail: led@kiku.dk.

‡ University of Copenhagen.

§ Present address: Institute of Chemistry, Leiden University, Einsteinweg 55, 2333 CC Leiden, The Netherlands.

|| Leiden University.

[1] Abbreviations: *Af*, *Alcaligenes faecalis* S-6; CPMG, Carr−Purcell−Meiboom−Gill; CT-CPMG, constant time CPMG; HSQC, heteronuclear single-quantum coherence; NIR, nitrite reductase; NMR, nuclear magnetic resonance; NOE, nuclear Overhauser effect; PAZ, pseudoazurin; PCu, plastocyanin; WT, wild-type.

10.1021/bi801858f CCC: $40.75
Published on Web 12/11/2008

MATERIALS AND METHODS

Protein Preparation. ^{15}N-labeled pseudoazurin from *A. faecalis* S-6 was produced and purified as previously described (*13*).

NMR Samples. All NMR samples contained 0.5 mM ^{15}N-labeled *Af* PAZ, 100 mM NaCl, and a 10% D_2O/90% H_2O mixture. Approximately 1 mM sodium ascorbate was added to reduce oxidized PAZ and maintain it in the reduced form. The pH was adjusted by adding small amounts of 1.0 M NaOH and HCl. All samples used in the relaxation measurements were sealed under a N_2 atmosphere. For the CPMG dispersion experiments, a sample with 20 mM phosphate and 20 mM acetate buffer was used. All other buffered PAZ solutions contained 10 mM phosphate and 10 mM deuterated acetate buffer. The mixed acetate/phosphate buffer was chosen to ensure pH stability over a broad range of pH values. The nonbuffered PAZ solutions were obtained by exchanging buffered PAZ solutions into a 100 mM NaCl solution.

NMR Experiments. NMR chemical shift titration experiments on ^{15}N-labeled *Af* PAZ were carried out on a Varian Inova 500 spectrometer operating at a magnetic field strength of 11.7 T, corresponding to a ^{1}H frequency of 499.97 MHz and a ^{15}N frequency of 50.67 MHz. The spectrometer was equipped with a highly sensitive cold probe. The pH dependence of the ^{15}N chemical shifts of the backbone amide groups was determined from a series of ^{15}N HSQC spectra recorded at 19 different pH values, using a standard gradient and a sensitivity-enhancing pulse sequence (*14*). The sweep widths in the ^{1}H and ^{15}N dimensions were 10000 and 2400 Hz, respectively; 1024 and 160 complex data points were acquired in the two dimensions, respectively. The resonance assignment of reduced *Af* PAZ has been published previously (*15*).

NMR relaxation experiments with [^{15}N]PAZ were carried out on a Varian Inova 800 spectrometer operating at a magnetic field strength of 18.7 T, corresponding to a ^{1}H frequency of 799.51 MHz and a ^{15}N frequency of 81.02 MHz. The spectrometer was equipped with a highly sensitive cold probe. Standard HSQC-based R_1 and R_2 experiments, as described by Farrow et al. (*16*), were conducted. Eight scans were acquired for each FID, using sweep widths of 11990 and 3400 Hz in the ^{1}H and ^{15}N dimensions, respectively; there were 2048 and 180 complex data points in the two dimensions, respectively. Each R_1 experiment consisted of eight spectra with different relaxation delays ranging from 0.01 to 1.9 s, while the R_2 experiments consisted of 11 spectra with relaxation delays ranging from 0.0 to 176 ms. In the ^{15}N R_2 experiments, a CPMG pulse was applied to the protons and the ^{15}N nuclei (*16*). The interpulse delay in the CPMG pulse was 8 ms for ^{1}H and 1 ms for ^{15}N.

^{15}N CT-CPMG experiments (*17*) were carried out at 11.7 T at five different temperatures from 5 to 25 °C. Constant time relaxation delays of 24, 24, 30, 48, and 60 ms were used at 5, 10, 15, 20, and 25 °C, respectively. There were 70 and 1024 complex data points in the ^{15}N and ^{1}H dimensions, respectively, recorded with 32 scans per FID for 18 CPMG field strengths, ν_{cpmg}, ranging from 40 to 1250 Hz. No measures were taken to compensate for sample heating by the CPMG pulse train; however, flat CPMG dispersion profiles were obtained for the majority of resonances, indicating that sample heating does not introduce any major artifacts.

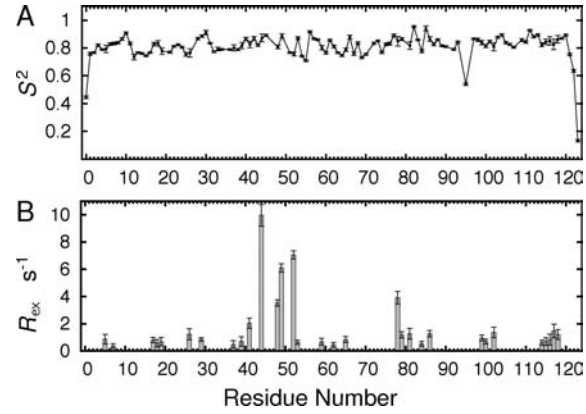

FIGURE 1: Model-free parameters of *Af* PAZ at 25 °C and pH 6 in the presence of 10 mM acetate buffer and 10 mM phosphate buffer: (A) generalized order parameters, S^2, vs the amino acid sequence and (B) exchange contributions, R_{ex}, at a magnetic field strength of 18.7 T.

Model-Free Analysis. Standard model-free calculations were carried out as previously described (*18*) using ^{15}N R_2, R_1, and {^{1}H}−^{15}N NOE data obtained at 800 MHz.

Chemical Shift Analysis. The pH dependencies of the ^{15}N and ^{1}H chemical shifts of the backbone amide groups of PAZ were analyzed as previously described (*12*). Chemical shift titration curves were fitted to the observed chemical shifts, δ_{obs} (see Figure 2) using the equation

$$\delta_{obs} = \delta_0 + \sum_{i=1}^{N} \frac{\Delta\delta_i}{1 + 10^{pH - pK_{ai}}} \quad (1)$$

where N (0, 1, 2, or 3) is the number of titrating residues which affects the chemical shift of a given residue, $\Delta\delta_i$ is the chemical shift change associated with pK_{ai}, and δ_0 is the chemical shift of the deprotonated state with respect to all N titrating residues. Equation 1 assumes that all titrations are independent of each other.

Determination of Exchange Rates. The exchange rate constant, k_{ex}, for the exchange between protonated and deprotonated His81 was determined from ^{15}N exchange contributions, R_{ex}, which in turn were derived from the ^{15}N R_2 and R_1 relaxation rates. The exchange contribution, R_{ex}, was determined from the R_2 and R_1 relaxation rates as previously described (*12*, *19*), using the approximation

$$R_{ex} = R_2 - R_1\left\langle \frac{R_2}{R_1} \right\rangle + \Delta_i \quad (2)$$

where Δ_i is a correction term, which compensates for errors introduced by picosecond to nanosecond internal dynamics (*12*, *19*). The Δ_i was calculated from the model-free parameters obtained above at pH 6, assuming that the picosecond to nanosecond dynamics is independent of pH. The R_{ex} contributions arising from protonation and deprotonation of His81 were analyzed according to a two-site exchange:

$$PH^+ \rightleftarrows D + H^+ \quad (3)$$

where PH^+ and D refer to the protonated and deprotonated forms, respectively. The exchange rate constant, k_{ex}, was obtained using the fast exchange equation

$$R_{ex} = \Delta\delta^2 a_{ex} \quad (4)$$

$$a_{ex} = \gamma^2 B_0{}^2 p_P p_D \frac{1}{k_{ex}}\left[1 - \frac{4\nu_{cpmg}}{k_{ex}} \tanh\left(\frac{k_{ex}}{4\nu_{cpmg}}\right)\right] \quad (5)$$

$$p_P p_D = (2 + 10^{pH-pK_a} + 10^{pK_a-pH})^{-1} \quad (6)$$

where $\Delta\delta$ is the chemical shift difference between the His81 protonated form, A, and the deprotonated form, B, a_{ex} is the exchange factor, and p_P and p_D are the populations of P and D, respectively. Furthermore, B_0 is the magnetic field strength, γ the gyromagnetic ratio, and ν_{cpmg} the radio frequency field strength of the CPMG pulse train applied on ^{15}N nuclei in the R_2 experiment. $\Delta\delta$ and pK_a were obtained from the chemical shift titration. Hence, eq 4 can be solved with respect to k_{ex}. A detailed description of the used method has been described previously (*12*).

Fitting of CPMG Dispersion Curves. CPMG dispersion curves were fitted numerically using the modified Bloch−McConnel equations for a two-site exchange process (*20*).

RESULTS

Model-Free Analysis of PAZ. ^{15}N R_2, R_1, and {^{1}H}−^{15}N NOE values were obtained for all previously assigned non-proline PAZ residues (*15*) at a magnetic field strenght of 18.7 T and at 25 °C and pH 6.0 in the presence of 10 mM acetate buffer and 10 mM phosphate buffer. Assuming isotropic rotational diffusion, the calculation resulted in a rotational correlation time of 7.17 ns, in good agreement with the molecular mass of PAZ. Calculations that were conducted using an anisotropic axially symmetric diffusion tensor did not improve the fit significantly compared to the isotropic model, according to F testing. Model-free parameters, S^2, R_{ex}, and τ_i, were therefore obtained using the isotropic rotational diffusion model. Order parameters, S^2, and exchange contributions, R_{ex}, are shown in Figure 1. The average order parameter is 0.82 excluding the C-terminus from the average. Exchange contributions were obtained for 32 residues and indicate the presence of micro- to millisecond conformational exchange processes in PAZ. As shown below, some of the R_{ex} contributions are associated with the protonation of His81. However, at pH 6, most of the larger exchange contributions arise from other processes unrelated to His81 and the copper site of PAZ.

pH Dependance of the Amide Chemical Shifts. To characterize the pH-dependent micro- to millisecond dynamics of His81 by ^{15}N relaxation, we first determined the titration shifts, $\Delta\delta$, of the backbone amide nitrogen chemical shifts independently (*12*) (see eq 4). To that end, a series of HSQC spectra were recorded at different pH values. Most signals in the ^{15}N HSQC spectrum have significant pH-dependent chemical shifts (see Figure 2). The titration shifts were obtained from chemical shift titration curves obtained for all residues in PAZ. Titration curves of the Cu ligands and His6 are shown in Figure 3. The effects from protonation of the two titratable histidines, His6 and His81, can clearly be observed on the amide chemical shifts. The pK_a values obtained for His6 and His81 were 7.15 ± 0.01 and 4.71 ± 0.02, respectively, in agreement with previous studies (*21*). In addition, chemical shift changes caused by the titration of carboxylate groups are observed. Several of the carboxylate groups titrate in the same pH region as His81. Therefore, there is some uncertainty about the extent to which the observed chemical shift changes are caused by the titration of His81 or of carboxylate groups. In PCu, it was found that carboxylate titration has a substantially smaller effect on the chemical shifts, presumably because they are more solvent-exposed compared to the histidines (*22*). Moreover, the distributions of carboxylate groups in PAZ and PCu are very different. Still, if the chemical shift changes associated with a pK_a value of 4.5−4.9 are compared with the corresponding chemical shift changes in PCu, the values are remarkably similar for the C-terminal copper binding loop (see Figure 4). Therefore, the chemical shift changes observed close to His81 can be affected only slightly by the titration of carboxylate groups, and we conclude that the chemical shift changes observed here are indeed caused primarily by the His81 titration.

pH-Dependent Micro- to Millisecond Dynamics in PAZ. The R_2 and R_1 relaxation rates were determined for all backbone ^{15}N atoms in PAZ that were observed in the ^{15}N HSQC spectrum. The rates were obtained at a field strength of 18.7 T using a buffered sample. At each pH value, the

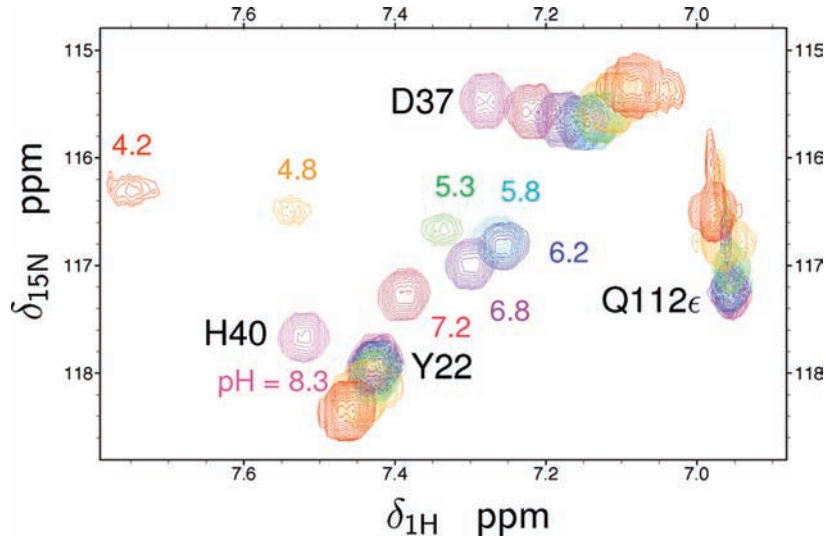

FIGURE 2: Excerpt of the 500 MHz HSQC spectrum of pseudoazurin at different pH values. The base level of the spectra at pH 4.8 and 4.2 is lowered by a factor 2.5 compared to the other spectra.

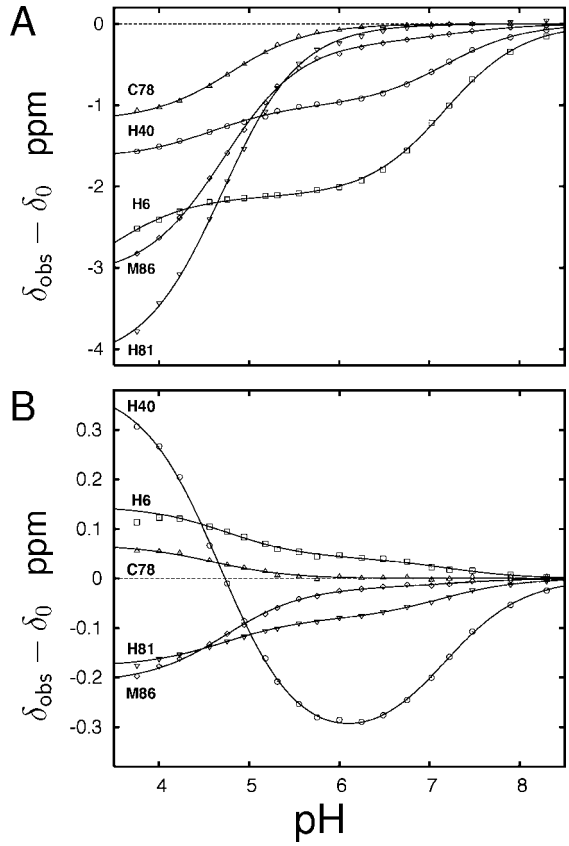

FIGURE 3: Chemical shift titration curves of the four copper-ligating residues and His6: (A) backbone ^{15}N titration curves and (B) backbone amide ^{1}H titration curves. The chemical shift, δ_0, corresponds to the fully deprotonated state.

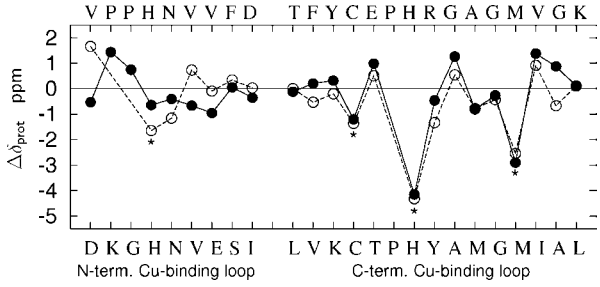

FIGURE 4: Comparison of the backbone ^{15}N chemical shift changes in the two copper-binding loops upon protonation of the C-terminal copper binding histidine in PAZ (●) (this work) and PCu (○) (*12*). Asterisks mark the copper-binding residues. The amino acid sequences of the copper binding loops of PAZ and PCu are given below and above the plot, respectively.

R_{ex} contributions were estimated from the R_2 and R_1 rates using eq 2, where the Δ_i corrections were calculated from the model-free parameters of PAZ as detailed previously (*12*, *19*). The obtained R_{ex} estimates were used to evaluate the pH-dependent micro- to millisecond dynamics in PAZ (see Figure 5). It was found that the majority of residues in PAZ have no significant R_{ex} contributions ($R_{ex} < 0.5\ s^{-1}$). Also the R_2/R_1 ratios of these residues are independent of pH, which indicates that the changes in pH do not lead to formation of oligomers that could complicate the analysis.

As in PCu, most residues close to the Cu(I) site exhibit pH-dependent exchange contributions. However, in contrast to the case for PCu, no linear correlation is observed between $|\Delta\delta_{prot}|$ and $\sqrt{R_{ex}}$ as shown in Figure 6. Also unlike the case for PCu, the pH dependence of R_{ex} is not the same for all residues as

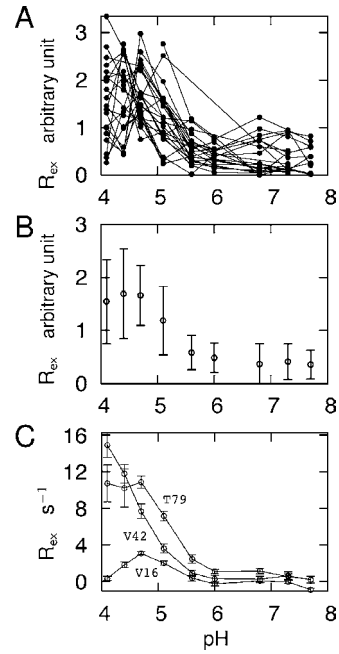

FIGURE 5: (A) pH dependencies of R_{ex} contributions in PAZ. The R_{ex} values were obtained at a field strength of 18.7 T using a buffered sample (10 mM acetate and 10 mM phosphate buffer). For each residue, the R_{ex} contributions are scaled by their average values over the pH interval from 4 to 8. (B) Average value of the scaled R_{ex} values shown in panel A. The error bars represent the standard deviation of the scaled R_{ex} values. (C) pH dependence of R_{ex} for three residues, V16, V42, and T79, close to the copper site and His81 in PAZ.

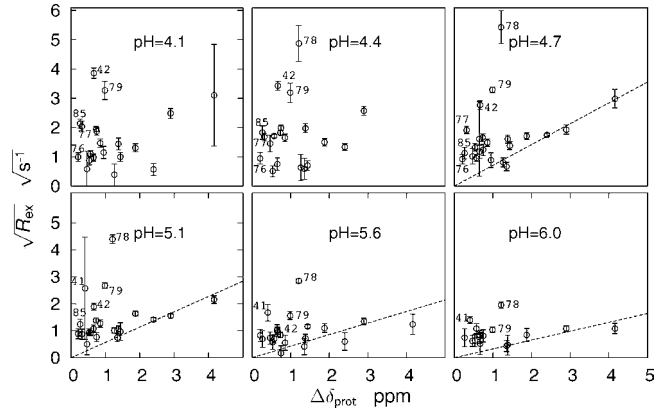

FIGURE 6: Square root of the pH-dependent R_{ex} contributions in PAZ vs the chemical shift change, $\Delta\delta_{prot}$, upon protonation of His81. The PAZ samples contained 10 mM acetate and 10 mM phosphate buffer. The R_{ex} values were obtained at a field strength of 18.7 T using a buffered sample. Plots are shown for six different pH values at 25 °C. The dashed lines represent the upper limit for exchange contributions caused by the protonation−deprotonation equilibrium (see the text). Data points representing residues that clearly contain an additional R_{ex} contribution are labeled by the residue number.

illustrated in panels A and C of Figure 5 (for comparison with PCu, see Figure 5 of ref *12*). Thus, for many residues, R_{ex} increases with a decrease in pH, and also at pH values below the pK_a value of His81. Only for a few residues does R_{ex} have a maximum when the pH is close to this pK_a. Taken together, this indicates that the exchange of His81 cannot be a simple two-site exchange process. A minimal model consistent with the observations requires at least one conformation in which His81 is deprotonated and two conformations in which His81 is protonated, as shown below.

Analyzing the R_{ex} Data Using a Simplified Three-Site Exchange Model. To analyze the pH-dependent exchange contribution, we approximate the multisite exchange process by two independent two-site processes. The first process is the exchange between two His81-protonated conformations (AH^+ and BH^+, eq 7 below) of the metal site of PAZ, and the second process is the exchange between the protonated conformations and deprotonated His81 (C, eq 7 below). In this model, the observed exchange contribution, R_{ex}, is the sum of the exchange contributions from the individual two-site exchange processes.

$$\begin{bmatrix} AH^+ \\ \uparrow\downarrow \\ BH^+ \end{bmatrix} \rightleftarrows C + H^+ \tag{7}$$

and

$$R_{ex} \approx a_{AB}\Delta\delta_{AB}{}^2 + a_{prot}\Delta\delta_{prot}{}^2 \tag{8}$$

where the exchange factors a_{AB} and a_{prot} are assumed to be independent of chemical shifts and depend on the chemical rate constants. Furthermore, $\Delta\delta_{AB}$ is the difference between the chemical shifts of the two protonated forms, AH^+ and BH^+, and $\Delta\delta_{prot}$ is difference between the chemical shifts of the deprotonated form and the population average of AH^+ and BH^+. This approximation simplifies the analysis and allows us to estimate the time scale of the processes. A similar approach in which a multisite exchange process is reduced to a sum of two effective two-site exchange processes has previously been employed by Malmendal et al. (*23*) and Grey et al. (*20*). In our study, a numerical simulation of the Bloch−McConnell equations of the full three-site exchange process confirmed that the approximated model is successful in describing qualitatively the overall behavior of R_{ex} as function of pH, buffer concentration, or CPMG frequency. However, the simulations also show that only for certain ranges of the parameters can the two-site approximation account quantitatively for the exchange contributions caused by the three-site process. Therefore, rate constants and chemical shifts obtained using this simplified model are effective, apparent values and should be interpreted with care.

Buffer-Dependent Exchange in PAZ. Buffers will enhance the rate of exchange between protonated and deprotonated His81, if the rate of interconversion is limited by the proton transfer. This was observed for the corresponding histidine residue in PCu (*9*) and in amicyanin (*5*). Thus, the difference, ΔR_{ex}, between the R_{ex} contributions obtained for PAZ in the presence and absence of buffer will be an increase in the exchange contribution associated with the protonation−deprotonation equilibrium, according to the approximation (eq 8). Since the rotational correlation time remains unchanged upon the removal of buffer, other contributions to the experimental R_2 rate are unaffected by the buffer. Therefore, ΔR_{ex} was obtained directly as the difference in R_2; that is, $\Delta R_{ex} = R_2^{nb} - R_2^{b}$, where R_2^{nb} and R_2^{b} are the R_2 rates in the absence and presence of buffer, respectively.

Significant ΔR_{ex} values are observed for many residues. The most conspicuous characteristic of the ΔR_{ex} values is that they correlate with the chemical shift differences, $\Delta\delta$, as shown in Figure 7. Furthermore, the slope reaches a maximum value at a pH close to the pK_a value of His81.

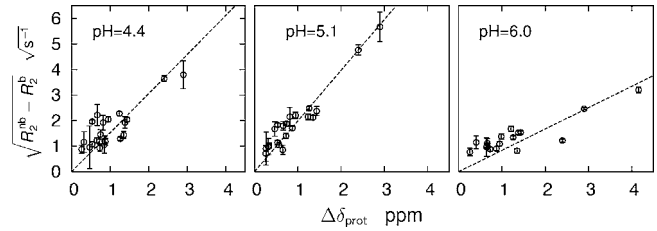

FIGURE 7: Square root of the difference in R_2 rates in PAZ in the presence of 10 mM acetate and 10 mM phosphate buffer and in the absence of buffer vs $\Delta\delta_{prot}$. Plots are shown for three different pH values. Dashed lines represent the least-squares linear fit.

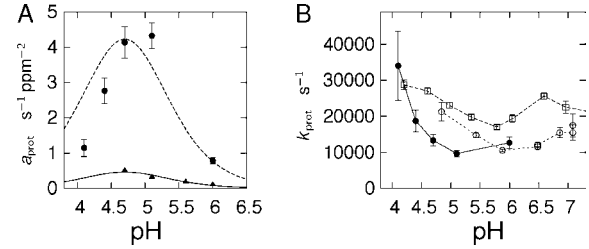

FIGURE 8: (A) Exchange factor a_{prot} for the protonation of His81 in PAZ vs pH in the presence of 10 mM acetate and 10 mM phosphate buffer (▲) and in the absence of buffer (●). The solid line represents the best fit to a_{prot} in the presence of buffer assuming a pH-independent exchange rate. The dotted line is the fit to a_{prot} in the absence of buffer assuming a pH-independent exchange rate. (B) k_{prot} values obtained from the a_{prot} values in the absence of buffer for PAZ (●) and the corresponding values previously obtained for WT PCu (□) and the PCu H61N mutant (○) (*9*).

These characteristics of the ΔR_{ex} values parallel those of the exchange contributions caused by a two-site exchange process between a protonated and deprotonated form (*12*, *24*) and support the notion that the two-site model (see eq 8) is indeed reasonable in this case and, thus, the effect from the protonation equilibrium can be separated from the equilibrium between different protonated forms of His81.

The slopes obtained from the fits in Figure 7 are given by $\sqrt{\Delta a_{prot}}$, where $\Delta a_{prot} = a_{prot}^{nb} - a_{prot}^{b}$, and a_{prot}^{nb} and a_{prot}^{b} are the a_{prot} values in the absence and presence of buffer, respectively. The factor a_{prot}^{b} was estimated at pH 4.7, 5.1, 5.6, and 6.0 using only the third of the data, which correspond to the smallest $R_{ex}/\Delta\delta_{prot}{}^2$ values (see Figure 6). According to eq 8, these residues are those most likely to be affected only by the protonation equilibrium. Still they may contain small contributions from the exchange between AH^+ and BH^+, and therefore, the obtained a_{prot}^{b} values are upper estimates. In particular at a pH below the pK_a of His81, where R_{ex} contributions arising from the interconversion between AH^+ and BH^+ are largest (see eq 7), the estimates of a_{prot}^{b} are unreliable. Therefore, at the two lowest pH values (pH 4.1 and 4.4), a_{prot}^{b} was extrapolated from the values obtained at the higher pH, assuming a pH-independent exchange rate, k_{prot}. Possible errors in the estimates of a_{prot}^{b} will, however, have little effect on the estimates of a_{prot}^{nb} because the a_{prot}^{b} values are small compared to the a_{prot}^{nb} values (Figure 8A and Table 1). Finally, the exchange rates, k_{prot}, in the absence and presence of buffer were calculated from the a_{prot}^{nb} and a_{prot}^{b} values, respectively, using eq 5. The obtained exchange rates, k_{prot}, in the absence of buffer range from 10000 to 40000 s^{-1} in the investigated pH range from pH 6 to 4 (see Figure 8B). In the presence of buffer, much faster k_{prot} rates that range from 110000 to 160000 s^{-1} are obtained (see Table 1).

Table 1: Exchange Factors and Exchange Rates Associated with the Protonation of His81 in the Presence and Absence of Buffer at Different pH Values

pH	a^{b}_{prot} (s^{-1} ppm^{-2})	Δa_{prot} (s^{-1} ppm^{-2})	a^{nb}_{prot} (s^{-1} ppm^{-2})	k^{b}_{prot} (s^{-1})	k^{nb}_{prot} (s^{-1})
4.1	0.30[a]	0.85	1.15	137000[a]	34000
4.4	0.41[a]	2.34	2.75	137000[a]	18700
4.7	0.51	3.67	4.18	125000	13350
5.1	0.32	3.94	4.26	163000	9700
5.6	0.18	nd[b]	nd[b]	140000	nd[b]
6.0	0.11	0.70	0.81	110000	12700

[a] Extrapolated values assuming k_{ex} is independent of pH. [b] Not determined.

Buffer-Independent Exchange at the Cu(I) Site of PAZ. Buffer-independent exchange processes in PAZ were studied at pH 5.1 using ^{15}N CPMG dispersion experiments at five different temperatures from 5 to 25 °C in the presence of 20 mM phosphate buffer and 20 mM acetate buffer. At this high buffer concentration, the protonation is expected to be sufficiently fast to eliminate the buffer-dependent R_{ex} contributions arising directly from the protonation of His81. Still, at a magnetic field strength of 11.7 T, large CPMG dispersions are observed for several residues in the active site. However, residues like His81 and Met86, which exhibit the largest chemical shift changes upon protonation of His81, show no or very little dispersion. Thus, the buffer-dependent component of R_{ex} is efficiently quenched. According to the two-site model (eq 7), the process becomes effectively a two-site exchange process. Therefore, the CPMG dispersion profiles were analyzed using a two-site model, analogous to eqs 4 and 5, where the parameters $\Delta\delta$, $p_P p_D$, and k_{ex} are substituted with the effective parameters $\Delta\delta_{eff}$, $(p_A p_B)_{eff}$, and k_{ex}^{eff}, respectively.

At 25 °C, the dispersion curves observed for residues close to the active site are linear, indicating that the exchange rate is several thousands per second and that only two parameters can be obtained from the dispersion curves. At lower temperatures, the flattening of the dispersion curves at high CPMG frequencies becomes observable, and in this case, three parameters can be obtained. However, the effective R_2 rate depends on four parameters, namely, R_2^0, k_{ex}^{eff}, $(p_A p_B)_{eff}$, and $|\Delta\delta_{eff}|$, and all four parameters can be obtained only if the exchange process is in the slow exchange regime. However, even at the lowest temperature, none of the obtained dispersion profiles clearly indicate that the process has crossed the coalescence point (i.e., $k_{ex} = \Delta\omega$) for any nucleus and entered the slow exchange regime. This implies that the chemical shift difference cannot be obtained in a manner independent of the populations. Residues with well-resolved dispersion profiles at all temperatures, e.g., Thr79, are clearly in the fast exchange regime at all temperatures. This puts a limit on how skewed populations p_A and p_B can be. Thus, we find that the equilibrium constant K_{AB} ($=p_B/p_A$) must be in the range of 0.1−10. Since the populations could not be determined more accurately, K_{AB} was arbitrarily set to 1.0 at 5 °C in the following global analysis of the CPMG dispersion curves. To account for the temperature dependence of the population, K_{AB} was set to $\ln(K_{AB}) = -\Delta H°/R[(T_0 - T)/(T_0 T)]$, where $T_0 = 278$ K. Here, $\Delta H°$ does not have a straightforward physical interpretation. Also, it should be noted that the exchange process is "diluted" by the presence of the His81-deprotonated state, which at the applied pH is 72% populated. To account for this dilution in the framework of the two-site model, the effective product of populations (eq 5) was set to $(p_A p_B)_{eff} = (p_A + p_C)p_B$. Furthermore, the analysis assumes that $\Delta\delta$ and the observed pK_a value are independent of the temperature. Finally, the exchange rate is assumed to follow the Eyring equation [$k_{ex}^{eff} = kT/h \exp(\Delta S^{‡}/R) \exp(-\Delta H^{‡})/RT$].

On the basis of these assumptions, the dispersion curves of Lys38, Val42, Asn63, Tyr64, Lys77, Cys78, Thr79, and Gly85 at five different temperatures were fitted globally to the two-site model. The parameters optimized in the fit are the activation parameters $\Delta S^{‡}$ and $\Delta H^{‡}$, one effective parameter, $\Delta H°$, accounting for the temperature dependence of the population, the chemical shift difference, $|\Delta\delta_{eff}|$, for each residue, and the R_0^2 rate for each dispersion curve, 51 parameters in total. The fit (see Figure 9) shows that the dispersion profiles of all eight residues are consistent with this simple two-site model. The effective activation parameters obtained from the fit, $\Delta H^{‡}$ and $\Delta S^{‡}$, are 30 kJ/mol and −73 J mol^{-1} K^{-1}, respectively, and $\Delta H°$ is 45 kJ/mol. The exchange rates that can be calculated from the apparent activation parameters range from ∼1500 s^{-1} at 5 °C to ∼4000 s^{-1} at 25 °C. Although the order of magnitude of the rate constants is reliable, it should be noted that the rate constants are apparent rate constants obtained from fitting a two-state model. Only to the extent that the two-site model (eqs 7 and 8) is applicable do the rate constants correspond to the interconversion between conformations AH^+ and BH^+. As noted above, the dispersion profiles do not deviate significantly from the fast exchange approximation and do, therefore, not allow a reliable separation of the effective chemical shift difference, $|\Delta\delta_{eff}|$, from the populations. Consequently, only the product Φ_{eff} [$=\Delta\delta_{eff}^2(p_A p_B)_{eff}$] (see Figure 9) can be determined. The residues with the largest Φ_{eff} values are Asn41, Val42, Asn63, Tyr64, Lys77, Cys78, Thr79, and Gly85. The Φ_{eff} value is a qualitative measure of the exchange between sites AH^+ and BH^+; the larger the Φ_{eff} value, the more likely it is that $|\Delta\delta_{AB}|$ is large, and residues with large $|\Delta\delta_{AB}|$ values are likely to be those involved in the conformational exchange between sites AH^+ and BH^+. A more rigorous interpretation is not possible because the two-site approximations may not be valid for all residues, and $\Delta\delta_{eff}$ may not only reflect the difference in chemical shift between the two protonated sites, AH^+ and BH^+, but also depend on the chemical shift of the deprotonated state, C. Even if the populations of AH^+ and BH^+ were known, it would not be possible to disentangle the chemical shifts of all three sites unless the sign of the chemical shift difference $\Delta\delta_{AB}$ can be determined (*25*). As long as the sign remains unknown, the $|\Delta\delta_{AB}|$ value of each nucleus can assume one of two possible values. These two solutions can be substantially different in cases where the two-site approximation does not apply. Whether the two-site approximation applies can only be accessed if all rate constants and chemical shifts in the three-site system are known. This ambiguity could be resolved by determining the sign of $|\Delta\delta_{AB}|$ (*26*), which, in principle, could be done under conditions where sites AH^+ and BH^+ are the only significantly populated sites, that is, at low pH (pH <4) where His81 is fully protonated. This would enable a complete analysis of the dispersion data using the three-site

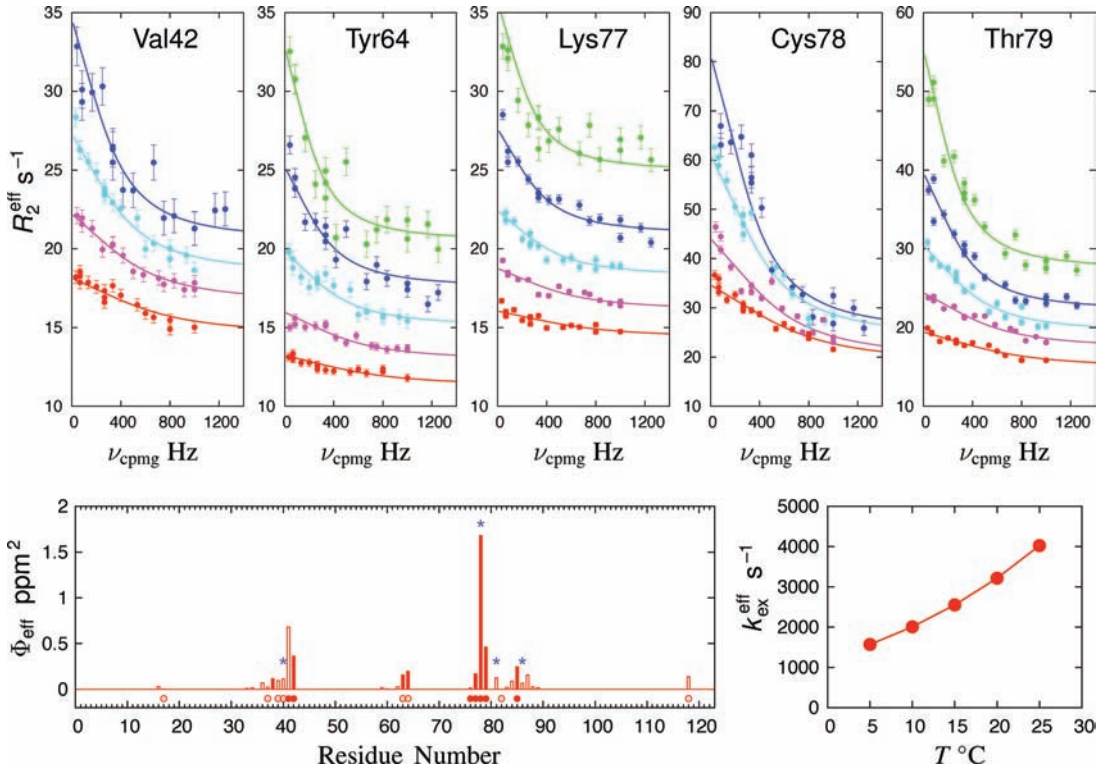

FIGURE 9: CPMG dispersion profiles (top panels) at different temperatures [5 (green), 10 (blue), 15 (cyan), 20 (magenta), and 25 °C (red)] of residues in the proximity of the copper site in PAZ. The dispersion curves were obtained at 11.7 T and pH 5.1 in the presence of 20 mM phosphate buffer and 20 mM acetate buffer to ensure that the protonation of His81 did not contribute directly to the dispersion. The lines represent a global fit. The bottom left panel shows the amplitudes of the CPMG dispersion profiles [$\Phi_{eff} = \Delta\delta_{eff}^2(p_A p_B)_{eff}$] at 5 °C vs the amino acid sequence of PAZ. Filled bars represent residues with unambiguous dispersion profiles, and empty bars represent data that are more tentative. Filled circles (●) mark residues with the largest $R_{ex}/\Delta\delta_{prot}^2$ ratios of >10 s^{-1} ppm^{-2}, and empty circles (○) mark residues with $R_{ex}/\Delta\delta_{prot}^2$ ratios between 2 and 10 s^{-1}ppm^{-2}. Asterisks mark the four copper ligands. The bottom right panel shows the effective exchange rates back-calculated from the fitted activation parameters vs temperature.

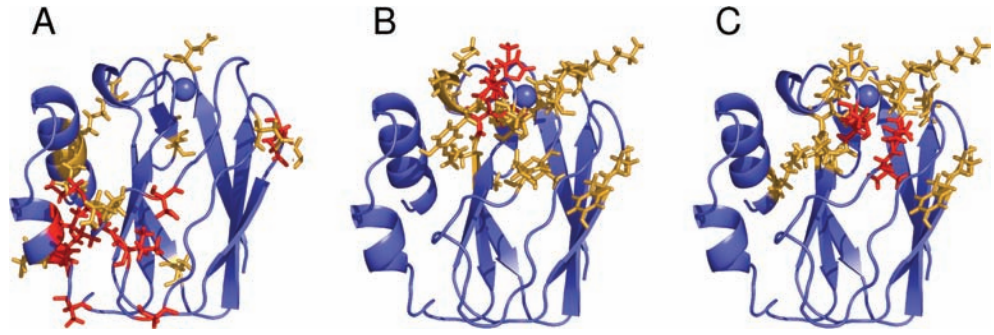

FIGURE 10: (A) Residues with R_{ex} contributions that are independent of pH: red for R_{ex} > 1 s^{-1} and orange for 0.5 s^{-1} < R_{ex} < 1 s^{-1}. (B) Residues affected by the protonation of His81 as indicated by residues with buffer-dependent R_{ex} values and large $\Delta\delta_{prot}$ values: red for $\Delta\delta_{prot}$ > 1.5 ppm and orange for 0.5 ppm < $|\Delta\delta_{prot}|$ < 1.5 ppm. (C) Residues affected by the exchange between different protonated forms of His81 as indicated by residues with significant pH-dependent but buffer-independent R_{ex} contributions. These residues are characterized by large Φ_{eff} [$=\Delta\delta_{eff}^2(p_A p_B)_{eff}$] values at 5 °C determined by CPMG dispersion: red for Φ_{eff} > 0.3 ppm^2 and orange for 0.03 ppm^2 < Φ_{eff} < 0.3 ppm^2.

model; unfortunately, the protein is not stable under the highly acidic conditions required for such an analysis.

pH-Independent Micro- to Milliscond Dynamics in PAZ. As shown by the R_{ex} terms obtained from a series of R_2 and R_1 experiments at different pH values, the exchange contributions for several residues are independent of pH in the observed pH range. Residues with pH-independent R_{ex} values of >1 s^{-1} are Ser44, Met48, Ile49, Gly52, Glu62, Ala97, Leu99, Ile102, and Ala120. Figure 10A shows the distribution of the residues on the structure. It is seen that the residues are mainly found in loop regions and in the nonsolvent exposed parts of the α-helices, whereas pH-independent exchange contributions are not observed for residues in the β-sheet core of the protein. Large CPMG dispersions are also observed for residues Ser44, Met48, and Ile49, and similar k_{ex} values were obtained for all three residues using the two-site model. However, the k_{ex} rates are ∼2 times smaller than the k_{ex} rates found in the proximity of the copper site. Therefore, these residues are involved in a different process, which is also apparent from the fact that this process is independent of pH and buffer concentration.

DISCUSSION

Pico- to Nanosecond Dynamics of Pseudoazurin. The dynamics on the pico- to nanosecond time scale of the

backbone of pseudoazurin resembles that of other blue copper proteins, such as azurin (*27*), plastocyanin (*18*, *28*), and rusticyanin (*29*), which all are highly rigid molecules on this time scale. Thus, for almost all residues, the order parameters are ~0.8, indicating that it is a highly rigid molecule, with little dynamics even in the loop regions. Only the residues at the termini and residue Ser95 have order parameters of <0.7.

Micro- to Millisecond Dynamics of Pseudoazurin. Whereas the backbone of PAZ is rigid on the pico- to nanosecond time scale, there are a variety of dynamics processes on the micro- to millisecond time scale which influence the ^{15}N R_2 rates. Thus, at 18.7 T, many residues are affected by conformational exchange on the micro- to millisecond time scale as indicated by the R_{ex} terms. The origins of the R_{ex} terms vary among the residues; however, the exchange contributions of PAZ can be separated into three groups (see Figure 10). (i) The first group consists of exchange contributions that are independent of pH (see Figure 10A). (ii) The second group includes exchange contributions that depend on the buffer concentration (see Figure 10B). These contributions stem from the protonation equilibrium of His81 and are observed for residues with large $\Delta\delta_{prot}$ values. (iii) The third group consists of exchange contributions that are pH-dependent but buffer-independent (see Figure 10C). These contributions are observed for residues with large values of $\Delta\delta_{AB}$ (see eq 8) and enhanced $R_{ex}/\Delta\delta_{prot}^2$ ratios and are caused by a yet unidentified exchange process within the active site of *Af* PAZ, a process that appears to be triggered by the protonation of His81. Residues in the third group also exhibit large CPMG dispersions at high buffer concentrations. Some residues with pH-independent motions (the first group) also exhibit CPMG dispersion, while others, like Gly52, do not. This suggests that there are several pH-independent exchange processes in PAZ.

Kinetics of the Protonation of His81. The exchange rates observed here for the exchange between the protonated and deprotonated His81 in PAZ are very similar to those measured for the corresponding process in PCu, suggesting that the protonation process is similar in the two proteins. Like in PCu, k_{prot} depends on pH and buffer concentration. This shows that the rate of protonation is limited by proton transfer at low buffer concentrations. Protonation requires that the imidazole ring first dissociate from the Cu(I) ion and then rotate ~180° around the $C^{\beta}-C^{\gamma}$ bond, making the $N^{\delta 1}$ atom surface exposed and thereby accessible to buffer ions. Inevitably, the rate of dissociation and rotation of the imidazole group must be equal to or faster than the fastest observed rate of exchange between protonated and deprotonated His81. Like in PCu (*9*), the exchange rates cannot be explained exclusively by specific acid−base catalysis (i.e., the protonation and deprotonation by the water solvent) in the case where no buffer is added, because this would give rise to unreasonably large second-order constants, close to or beyond the equivalent rate constants for protonation of free imidazole, a process known to be diffusion-limited (*30*). The PCu studies (*9*) suggest that the copper binding slows the proton transfer by 2−3 orders of magnitude, since the copper binding prevents the histidine from becoming protonated. Thus, realistic second-order rate constants for specific acid−base catalysis should be at least 2 orders of magnitude below the protonation−deprotonation rates of free imidazole which are 2×10^{10} M^{-1} s^{-1}. Possible explanations for the fast protonation and deprotonation may include the small amount of buffer remaining after dialysis or impurities from small amounts of denatured and hydrolyzed protein that contribute to the protonation rate.

Dynamics of His81-Protonated PAZ. An additional conformational exchange in the active site of PAZ occurs when His81 becomes protonated. According to the CPMG dispersion profiles this process is slower than the protonation equilibrium even at low buffer concentrations. This exchange is not observed in PCu, yet in amicyanin, an exchange process on a similar time scale has been reported (*5*). In the study of amicyanin, the authors suggested that the additional exchange may be an exchange between different orientations of the protonated imidazole ring. The same could be the case in PAZ. Such a rearrangement could be triggered by the binding of other ligands, such as a water molecule, which replace the imidazole group of His81. Although buffer molecules may also transiently bind to the Cu(I) ion, they cannot be responsible for the relaxation enhancements because the effect is also observed after the removal of buffers. However, the conformational exchange may also be a rearrangement of other residues proximal to the copper site. It is noteworthy that the residues in PAZ that are most affected by this process are Cys78 and residues Asn41, Val42, Lys77, and Thr79, all of which are close to the cysteine, whereas the backbone ^{15}N of His81 is only slightly affected. This could suggest that the observed conformational exchange is not a rearrangement of the protonated His81 side chain. The change from a tetrahedral to a planar trigonal geometry of the copper site triggered by the protonation of His81 may result in a rearrangement in the second coordination sphere. Structural changes in the second coordination sphere have been shown to cause sizable effects on the redox properties and pK_a value of copper sites in blue copper proteins (*31*, *32*). Such changes would most likely also effect the ^{15}N chemical shifts of residues in the proximity of the copper site and could explain the exchange broadening. Conformational fluctuations on the micro- to millisecond time scale are also observed near the Cu(I) site of azurin where the C-terminal histidine of azurin does not protonate (*33*, *34*). In azurin, this dynamics is likely to be associated with conformational changes of a histidine side chain, His35, in the vicinity of the copper site, a residue that is absent in PAZ and amicyanin. In PAZ, as judged from the residues with the largest relaxation effects, we speculate the rearrangement could involve Cys78 and its hydrogen bonding interactions with Asn41.

ACKNOWLEDGMENT

We thank Malene R. Jensen, D. Flemming Hansen, and Søren M. Kristensen for helpful discussions and Robert Dagil, Lise-Lotte Jespersen, Jens Ø. Duus, and Bent O. Petersen for technical assistance. The 800 MHz spectra were acquired at The Danish Instrument Center for NMR Spectroscopy of Biological Macromolecules.

SUPPORTING INFORMATION AVAILABLE

Tables with chemical shift titration parameters, model-free parameters, and plots showing additional CPMG disper-

sion profiles of *Av* PAZ. This material is available free of charge via the Internet at http://pubs.acs.org.

REFERENCES

1. Petratos, K., Dauter, Z., and Wilson, K. S. (1988) Refinement of the structure of pseudoazurin from *Alcaligens faecalis* S-6 at 1.55 Å resolution. *Acta Crystallogr. B44*, 628–636.
2. Dennison, C., Kohzuma, T., McFarlane, W., Suzuki, S., and Sykes, A. G. (1994) Reactivity of pseudoazurin from *Achromobacter cycloclastes* with inorganic redox partners and related NMR and electrochemical studies. *Inorg. Chem. 33*, 3299–3305.
3. Guss, J. M., Harrowell, P. R., Murata, M., Norris, V. A., and Freeman, H. C. (1986) Crystal structure analyses of reduced (Cu^I) poplar plastocyanin at six pH values. *J. Mol. Biol. 192*, 361–387.
4. Lommen, A., Canters, G. W., and van Beeumen, J. (1988) A ^{1}H-NMR study on the blue copper protein amicyanin from *Thiobacillus versutus*. Resonance identifications, structural rearrangements and determination of the electron self-exchange rate constant. *Eur. J. Biochem. 176*, 213–223.
5. Lommen, A., and Canters, G. W. (1990) pH-dependent redox activity and fluxionality of the copper site in amicyanin from *Thiobacillus versutus* as studied by 300- and 600-MHz ^{1}H NMR. *J. Biol. Chem. 265*, 2768–2774.
6. Battistuzzi, G., Borsari, M., Canters, G. W., de Waal, E., Leonardi, A., Ranieri, A., and Sola, M. (2002) Thermodynamics of the acid transition in blue copper proteins. *Biochemistry 41*, 14293–14298.
7. Battistuzzi, G., Borsari, M., Loschi, L., Ranieri, A., Sola, M., and Mondovì, A. M. B. (2001) Redox properties and acid−base equilibria of zucchini mavicyanin. *J. Inorg. Biochem. 83*, 223–227.
8. Markley, J. L., Ulrich, E. L., Berg, S. P., and Krogmann, D. W. (1975) Nuclear magnetic resonance studies of copper binding sites of blue copper proteins: Oxidized, reduced, and apoplastocyanin. *Biochemistry 14*, 4428–4433.
9. Hass, M. A. S., Christensen, H. E. M., Zhang, J., and Led, J. J. (2007) Kinetics and mechanism of the acid transition of the active site in plastocyanin. *Biochemistry 46*, 14619–14628.
10. Kramer, D. M., Sacksteder, C. A., and Cruz, J. A. (1999) How acidic is the lumen? *Photosynth. Res. 60*, 151–163.
11. Canters, G. W., Kolczak, U., Armstrong, F., Jeuken, L. J. C., Camba, R., and Sola, M. (2000) The effect of pH and ligand exchange on the redox properties of blue copper proteins. *Faraday Discuss. 116*, 205–220.
12. Hass, M. A. S., Thuesen, M. H., Christensen, H. E. M., and Led, J. J. (2004) Characterization of μs−ms dynamics of proteins using a combined analysis of ^{15}N NMR relaxation and chemical shift: Conformational exchange in plastocyanin induced by histidine protonations. *J. Am. Chem. Soc. 126*, 753–765.
13. Vlasie, M., Comuzzi, C., van den Nieuwendijk, A. M., Prudencio, M., Overhand, M., and Ubbink, M. (2007) Long-range-distance NMR effects in a protein with a lanthanide-DOTA chelate. *Chemistry 13*, 1715–1723.
14. Zhang, O., Kay, L. E., Olivier, J. P., and Forman-Kay, J. D. (1994) Backbone ^{1}H and ^{15}N resonance assignments of the N-terminal SH3 domain of drk in folded and unfolded states using enhanced-sensitivity pulsed field gradient NMR techniques. *J. Biomol. NMR 4*, 845–858.
15. Impagliazzo, A., and Ubbink, M. (2004) ^{1}H, ^{13}C and ^{15}N resonance assignment of Cu(I)-pseudoazurin from *Alcaligenes faecalis* S-6. *J. Biomol. NMR 29*, 541–542.
16. Farrow, N. A., Muhandiram, R., Singer, A. U., Pascal, S. M., Kay, C. M., Gish, G., Shoelson, S. E., Pawson, T., Forman-Kay, J. D., and Kay, L. E. (1994) Backbone dynamics of free and a phosphopeptide-complexed Src homology 2 domain studied by ^{15}N NMR relaxation. *Biochemistry 33*, 5984–6003.
17. Tollinger, M., Skrynnikov, N. R., Mulder, F. A. A., Forman-Kay, J. D., and Kay, L. E. (2001) Slow dynamics in folded and unfolded states of an SH3 domain. *J. Am. Chem. Soc. 123*, 11341–11352.
18. Ma, L., Hass, M. A. S., Vierick, N., Kristensen, S. M., Ulstrup, J., and Led, J. J. (2003) Backbone dynamics of reduced plastocyanin from the cyanobacterium *Anabaena variabilis*: Regions involved in electron transfer have enhanced mobility. *Biochemistry 42*, 320–330.
19. Hass, M. A. S., and Led, J. J. (2006) Evaluation of two simplified N-15-NMR methods for determining μs-ms dynamics of proteins. *Magn. Reson. Chem. 44*, 761–769.
20. Grey, M. J., Wang, C., and Palmer, A. G. (2003) Disulfide Bond Isomeration in Basic Pancreatic Trypsin Inhibitor: Multisite Chemical Exchange Quantified by CPMG Relaxation Dispersion and Chemical Shift Modeling. *J. Am. Chem. Soc. 125*, 14324–14335.
21. Impagliazzo, A., Blok, A. J., Cliff, M. J., Ladbury, J. E., and Ubbink, M. (2007) Redox-State-Dependent Complex Formation between Pseudoazurin and Nitrite Reductase. *J. Am. Chem. Soc. 129*, 226–233.
22. Hass, M. A. S., Jensen, M. R., and Led, J. J. (2008) Probing electric fields in proteins by NMR. *Proteins 72*, 333–343.
23. Malmendal, A., Evenäs, J., Forsén, S., and Akke, M. (1999) Structural dynamics in the C-terminal domain of calmodulin at low calcium levels. *J. Mol. Biol. 293*, 883–899.
24. Sudmeier, J. L., Evelhoch, J. L., and Jonsson, N. B.-H. (1980) Dependence of NMR lineshape analysis upon chemical rates and mechanisms: Implications for enzyme histidine titrations. *J. Magn. Reson. 40*, 377–390.
25. Hass, M. A. S., Hansen, D. F., Christensen, H. E. M., Led, J. J., and Kay, L. E. (2008) Characterization of conformational exchange of a histidine side chain: Protonation, rotamerization and tautomerization of His61 in plastocyanin from *Anabaena variabilis*. *J. Am. Chem. Soc. 130*, 8460–8470.
26. Skrynnikov, N. R., Dahlquist, F. W., and Kay, L. E. (2002) Reconstructing NMR spectra of "invisible" exited protein states using HSQC and HMQC experiments. *J. Am. Chem. Soc. 124*, 12352–12360.
27. Kalverda, A. P., Ubbink, M., Gilardi, G., Wijmenga, S. S., Crawford, A., Jeuken, L. J. C., and Canters, G. W. (1999) Backbone dynamics of azurin in solution: Slow conformational change associated with deprotonation of histidine 35. *Biochemistry 38*, 12690–12697.
28. Bertini, I., Bryant, D. A., Ciurli, S., Dikiy, A., Fernández, C. O., Luchinat, C., Safarov, N., Vila, A. J., and Zhao, J. (2001) Backbone dynamics of plastocyanin in both oxidation states. *J. Biol. Chem. 276*, 47217–47226.
29. Jiménez, B., Piccioli, M., Moratal, J.-M., and Donaire, A. (2003) Backbone dynamics of rusticyanin: The high hydrophobicity and rigidity of this blue copper protein is resposible for its thermodynamic properties. *Biochemistry 42*, 10396–10405.
30. Eigen, M. (1963) Protonenübertragung, Säure-Base-Katalyse und enzymatische Hydrolyse. Teil I: Elementarvorgänge. *Angew. Chem. 75*, 489–508.
31. Yanagisawa, S., Crowley, P. B., Firbank, S. J., Lawler, A. T., Hunter, D. M., McFarlane, W., Li, C., Kohzuma, A., Banfield, M. J., and Dennison, C. (2008) π-interaction tuning of the active site properties of metalloproteins. *J. Am. Chem. Soc. 130*, 15420–15428.
32. Li, C., Banfield, M. J., and Dennison, C. (2007) Engineering copper sites in proteins: Loops confer native structures and properties to chimeric cupredoxins. *J. Am. Chem. Soc. 129*, 709–718.
33. Korzhnev, D. M., Karlsson, B. G., Orekhov, V. Y., and Billeter, M. (2003) NMR detection of multiple transitions to low-populated states in azurin. *Protein Sci. 12*, 56–65.
34. Zhuravleva, A. V., Korzhnev, D. M., Kupce, E., Arseniev, A. S., Billeter, M., and Orekhov, V. Y. (2004) Gated electron transfers and electron pathways in azurin: A NMR dynamics study at multiple fields and temperatures. *J. Mol. Biol. 342*, 1599–1611.

BI801858F